International Journal of Science & Technology (PRAGYANAM)
Volume 1 • Issue 1 • January–December 2025
ISSN:

# Nickel-Based Nanocomposites with Tunable Optical Properties for Sustainable Solar Energy Solutions

**Soumya Rai[1], Himani Chaudhary[2], Peeyush Phogat[3], Shreya[4], Ranjana Jha[5] & Sukhvir Singh[6]**

ABSTRACT

*The increasing global demand for efficient solar energy harvesting materials has fueled the development of innovative nanocomposites. Among these, Nickel hydroxide/nickel sulphide ($Ni(OH)_2$/NiS) and nickel oxide/nickel sulphide (NiO/NiS) nanocomposites hold great promise owing to their distinct structural and optical properties. These nanocomposites were synthesized using the hydrothermal method, a process that ensures uniformity and high-quality material production. Structural analysis via X-ray diffraction (XRD) revealed hexagonal crystalline structures for $Ni(OH)_2$ and NiS, while NiO exhibited a cubic structure. Morphological studies using Field Emission Scanning Electron Microscopy (FESEM) highlighted distinct features: 2D nanosheets were observed for $Ni(OH)_2$, NiO, and NiO/NiS, whereas $Ni(OH)_2$/NiS exhibited intriguing broccoli-like structures. Optical characterization through UV-Visible spectroscopy demonstrated a significant reduction in band gaps, from 4.4 eV for $Ni(OH)_2$ and 3.1 eV for NiO to 1.08 eV and 1.3 eV in their respective nanocomposites. This band gap narrowing enhances light absorption, making these materials highly suitable for solar energy applications. FT-IR analysis highlighted distinctive peaks especially in the fingerprint regions, such as the Ni-O vibrations and the C=S stretching, confirming the successful incorporation of NiS into the nanocomposites. These findings underline the potential of $Ni(OH)_2$/NiS and NiO/NiS nanocomposites as cost-effective and high-performance alternatives for solar cells, advancing sustainable energy technologies and opening the door to more effective photovoltaic systems.*

**Keywords:** Nickel Hydroxide, Nickel Oxide, Nickel Sulphide, Optical Properties, Solar Cells

## INTRODUCTION

The increasing requirement for renewable energy alternatives has driven significant research into advanced materials for solar cells, focusing on enhancing efficiency, stability, and cost-effectiveness. Scientists aim to develop innovative materials that not only improve energy conversion rates but also offer long-term durability and affordability. This endeavour is essential to reducing dependency on fossil fuels and supplying the world's energy demands in a sustainable manner and advancing the adoption of clean, renewable energy technologies [1]-[7]. Solar cells harness sunlight to generate electricity via the photovoltaic effect, a process that relies heavily on the properties of semiconducting materials. These materials are engineered to optimize light absorption, efficiently capturing solar energy, and to enhance charge carrier dynamics, ensuring effective separation

[1] Research Lab for Energy System, Department of Physics, Netaji Subhas University of Technology, New Delhi, India.
E-mail: soumyarai.sr16@gmail.com

[2] Research Lab for Energy System, Department of Physics, Netaji Subhas University of Technology, New Delhi, India.
E-mail: chnehasingh1998@gmail.com

[3] Research Lab for Energy System, Department of Physics, Netaji Subhas University of Technology, New Delhi, India.
E-mail: peeyush.phogat@gmail.com

[4] Research Lab for Energy System, Department of Physics, Netaji Subhas University of Technology, New Delhi, India.
E-mail: shreyasharma.aug15@gmail.com

[5] Research Lab for Energy System, Department of Physics, Netaji Subhas University of Technology, New Delhi, India.
E-mail: drranjanajha@gmail.com

[6] Research Lab for Energy System, Department of Physics, Netaji Subhas University of Technology, New Delhi, India.
E-mail: sukhvirster@gmail.com

and transport of holes and electrons. The performance of solar cells depends on the careful design and selection of these semiconductors to achieve high efficiency and sustainability [8]-[12]. Nickel-based compounds, particularly nickel hydroxide ($Ni(OH)_2$) and nickel oxide (NiO), have attracted a lot of interest because of their potential in energy applications and because of their distinct optical, electrochemical, and electronic characteristics. These compounds exhibit excellent catalytic activity, high stability, and efficient charge storage capabilities, rendering them appropriate for a range of uses, including energy storage devices, supercapacitors, batteries, and electrocatalysis. Their ability to facilitate efficient electron transfer and energy conversion processes positions them as promising materials for advancing sustainable energy technologies [13]-[16].

Nickel hydroxide ($Ni(OH)_2$), composed of nickel ($Ni^{2+}$) and hydroxide ($OH^-$) ions, is a versatile and widely utilized material in energy storage systems. It plays a crucial role in nickel-metal hydride (NiMH) batteries, where it serves as the active electrode material. Its high energy density, stability, and efficient charge-discharge characteristics make it essential for rechargeable battery technologies [17]. Its layered structure facilitates ion transport, making it a promising candidate for energy applications [18]-[22]. However, $Ni(OH)_2$ alone faces significant challenges when used in solar cell applications, such as low electrical conductivity, limited visible light absorption, and potential instability under operational conditions. These limitations make $Ni(OH)_2$ less effective as a photoactive material for efficient energy conversion in solar cells. The low conductivity hampers the efficient transport of charge carriers, while the restricted absorption of visible light reduces its overall performance in harnessing solar energy. Additionally, $Ni(OH)_2$'s susceptibility to degradation under varying environmental conditions can affect the longevity and stability of solar devices.

To address these drawbacks, $Ni(OH)_2$ can be thermally treated or calcined to form nickel oxide (NiO), a more robust and thermally stable material. NiO possesses a wide band gap and p-type semiconducting properties, which enhance its suitability for solar cell applications. These improvements in electrical and optical properties make NiO a more effective material for increasing the efficiency and stability of solar cells [23]-[27]. The transformation of nickel hydroxide ($Ni(OH)_2$) into nickel oxide (NiO) involves heating the material to remove water, resulting in a crystalline NiO structure with improved chemical stability and thermal resistance. NiO's wide band gap makes it a suitable material for charge transport layers in solar cells, enhancing efficiency in energy conversion. However, its limited absorption in the visible spectrum restricts its ability to function effectively as a standalone photoactive material. To address this challenge, researchers have focused on combining NiO with narrow-bandgap semiconductors to create hybrid nanocomposites. These hybrid structures aim to leverage the strengths of both materials, optimizing performance.

Nickel sulfide (NiS), known for its excellent visible light absorption and catalytic properties, has emerged as a promising candidate for these hybrid systems. By integrating NiS with NiO, these nanocomposites can potentially overcome the optical limitations of NiO, improving the efficiency of applications such as solar energy conversion [28]-[31]. The integration of NiS into $Ni(OH)_2$ or NiO matrices results in nanocomposites with synergistic properties, including enhanced light absorption in both UV and visible region and reduced energy bandgap. These enhancements are critical for achieving higher solar energy conversion efficiencies.

Recent studies have explored a wide range of materials to enhance the efficiency and cost-effectiveness of solar cells, focusing on perovskites [32]-[34], quantum dots [35]-[37], and metal oxides [38]-[40]. Perovskites have shown exceptional performance in solar cell applications due to their high-power conversion efficiencies, but their stability issues and potential toxicity present significant challenges for long-term use and commercial scalability [41]. Quantum dots, on the other hand, offer the advantage of tunable band gaps, allowing for precise control over the light absorption spectrum. However, their complex fabrication processes and potential issues with stability and scalability hinder their widespread application. Metal oxides including titanium dioxide ($TiO_2$) and zinc oxide (ZnO) are widely utilized as electron transport materials in solar cells. Although they offer good electron mobility and stability, they often lack sufficient light absorption properties in the visible range, limiting their overall efficiency in solar energy conversion[42]. These challenges continue to drive research into new,

more effective materials. Nickel-based materials are highly regarded for their environmental compatibility, cost-effectiveness, and ease of synthesis, making them excellent candidates for sustainable solar energy applications. Their abundant availability, low cost, and efficient performance in energy conversion processes ensure they are an attractive alternative to more expensive or environmentally harmful materials in solar technologies.

This study investigates the hydrothermal synthesis of nickel hydroxide ($Ni(OH)_2$) and its subsequent calcination to nickel oxide (NiO), followed by the integration of nickel sulfide (NiS) to form $Ni(OH)_2$/NiS and NiO/NiS nanocomposites. These nanocomposites are further investigated on the basis of their structural, optical, morphological and chemical properties. The combination of $Ni(OH)_2$ and NiO, both of which are known for their wide-bandgap stability, with NiS, a material renowned for its excellent visible light absorption and catalytic efficiency, results in the creation of advanced nanocomposites. These nanocomposites effectively address the limitations of each individual component, enhancing the overall performance of solar energy devices. The $Ni(OH)_2$/NiS and NiO/NiS nanocomposites exhibit enhanced optical absorption properties, particularly in the visible light spectrum, making them highly suitable for solar energy harvesting. Additionally, the materials show improved stability, crucial for long-term efficiency in photovoltaic applications. The synergistic effect between the components contributes to better charge separation and transport, leading to higher photocatalytic and photovoltaic performance compared to individual $Ni(OH)_2$, NiO, or NiS materials.

The study highlights that these nickel-based nanocomposites hold significant promise as cost-effective and sustainable solutions for next-generation solar cells. Their synthesis through a relatively simple hydrothermal method, followed by calcination, offers a scalable approach for large-scale production. The integration of NiS enhances the overall material properties, enabling the development of efficient photovoltaic materials that can contribute to the global transition towards cleaner, renewable energy sources. This work represents a significant step toward advancing solar technologies, positioning nickel-based nanocomposites as key materials for future energy harvesting systems.

## EXPERIMENTAL SECTION

### Chemicals Used

The chemicals and reagents used in the synthesis process are listed in Table 1, detailing their manufacturer names and purity percentages. Absolute ethanol and de-ionized (DI) water with a resistivity greater than 5M were utilized for synthesis and cleaning steps, ensuring high-quality and contamination-free results. These high-purity solvents played a crucial role in the preparation of the nanocomposites, maintaining the integrity of the experimental procedure and contributing to reliable and reproducible outcomes.

**Table 1.** Chemicals used in the synthesis process

| *Chemical Name* | *Chemical Formula* | *Manufacturer Company* | *Purity* |
|---|---|---|---|
| Nickel Nitrate Hexahydrate | $Ni(NO_3)_2 \cdot 6H_2O$ | M/s Thomas Baker | 99% |
| Sodium Hydroxide | NaOH | M/s Thomas Baker | 99% |
| Sodium Sulphide | $Na_2S$ | M/s Thomas Baker | 98% |

### Synthesis Process

A simple and efficient single-step hydrothermal synthesis method was employed to fabricate the materials. Nickel hydroxide ($Ni(OH)_2$) was synthesized by dissolving 0.27 M nickel nitrate hexahydrate in 40 mL of de-ionized (DI) water under continuous magnetic stirring for 30 minutes at room temperature, ensuring complete dissolution and uniformity of the solution. In a separate step, a 2.0 M sodium hydroxide (NaOH) solution was made starting with dissolving 2 grams NaOH in 25 mL DI water and stirring the solution for 30 minutes to achieve a homogeneous mixture. The NaOH solution was then introduced dropwise to the nickel nitrate solution under continuous stirring to facilitate controlled precipitation. This was followed by 3 hours of additional stirring to promote the formation of uniform nanoparticles. After that, the mixture was moved to a Teflon-lined stainless-steel autoclave and heated hydrothermally at 220°C for 24 hours. After the reaction, the resulting particles were collected by centrifugation, which were then repeatedly cleaned with ethanol and DI water to get

rid of contaminants, dried in a vacuum oven at 60°C to ensure even dehydration, and then crushed into a fine powder. This sample, designated as NB (color-coded blue), represented pure $Ni(OH)_2$.

To convert nickel hydroxide into nickel oxide (NiO), sample NB was calcined at 350°C for 1 hour. This thermal treatment resulted in sample NA, which was color-coded pink. For the synthesis of $Ni(OH)_2$/NiS nanocomposites, 0.17 M of sample NB was dispersed in 15 mL DI and mixed for 30 minutes to ensure uniform dispersion. Simultaneously, a 0.17 M sodium sulfide ($Na_2S$) solution was prepared and added dropwise to the $Ni(OH)_2$ suspension under continuous stirring for 3 hours to facilitate the interaction and formation of the nanocomposite. After that, the mixture was placed in an autoclave and hydrothermally treated for 24 hours at 220°C. The final product was washed, dried, and ground into a uniform powder, resulting in the sample NB/NS, color-coded red. Using a similar procedure, sample NA was used instead of NB to prepare NiO/NiS nanocomposites, designated as NA/NS and color-coded green. This approach ensured precise control over material properties, enabling their application in advanced energy and catalytic technologies.

## RESULTS AND DISCUSSON

### X-Ray Diffraction

An advanced analytical model, Expert PRO X-Ray Diffractometer, equipped with copper Kα radiation (wavelength 1.54 Å), was employed to investigate the structural properties of the synthesized samples. The XRD patterns recorded across a wide 2θ range of 10° to 90°, captured detailed crystallographic information, as illustrated in fig. 1, which also includes the corresponding matched JCPDS file numbers. Sample NB exhibited a well-defined hexagonal crystal structure characteristic of $Ni(OH)_2$. However, upon calcination at 350°C, the crystal structure underwent a transformation to a cubic phase, as observed in sample NA. This structural transition can be attributed to the thermal energy provided during calcination, which rearranged the nickel and oxygen ions. The process caused a transition from a layered hydroxide structure to a more compact and thermodynamically stable cubic NiO phase. At elevated temperatures, the cubic structure of NiO is inherently more stable, driving this transformation.

The incorporation of nickel sulfide (NiS) into the matrices of $Ni(OH)_2$ and NiO further modified the structural properties, as observed in the XRD patterns of samples NB/NS and NA/NS. The inclusion of NiS introduced additional diffraction peaks, indicative of the formation of new crystallographic phases within the composites. This likely reflects enhanced crystallinity, improved atomic ordering, and a reduction in structural defects. The crystallographic interactions between NiS and the host matrices appeared to strengthen the material's structural integrity, with better atomic alignment and reduced disorder. These modifications, as evident from the additional peaks in the XRD patterns, indicate improved charge transport and enhanced light absorption properties. These characteristics make the NiS-based nanocomposites highly promising candidates for advanced solar cell applications, showcasing their potential for efficient energy conversion in sustainable energy solutions.

The Debye-Scherrer equation is important for determining the crystallite size of materials from X-ray diffraction (XRD) patterns. It provides insights into the structural characteristics of nanoparticles, helping to quantify their size and assess the material's quality. This information is crucial for understanding the material's properties, such as its optical, electrical, and mechanical behavior. The Debye-Scherrer equation was utilised to assess the size of the crystallites of the as-synthesized samples [43]-[46] as given by equation-1,

$$d = K\frac{\lambda}{\beta \cos\theta} \quad \ldots(1)$$

Here, d denotes the average size of crystallite, value of shape constant K is 0.9, λ depicts the wavelength of x-ray (1.54 Å), β specifies the full width at half maxima (FWHM), θ refers to the Bragg's angle of corresponding peaks [50], [51]. The average crystallite sizes for samples NB, NA, NB/NS, and NA/NS were computed using the formula and the values are depicted in Table 2. The reduction in crystallite size observed from NB to NA upon calcination is primarily attributed to the decomposition of hydroxide layers in $Ni(OH)_2$ and the subsequent reorganization of atoms during the thermal process. This transformation leads

to the separation of atoms and restricts extensive grain growth, resulting in a smaller crystallite size in the calcined sample (NA).

The calcination process causes the transition from a layered hydroxide structure to a more compact, thermodynamically stable cubic NiO phase, which further limits the growth of crystallites. In contrast, the incorporation of nickel sulfide (NiS) into both NB and NA matrices results in an increase in crystallite size, as observed in the NB/NS and NA/NS nanocomposites. This increase in size is likely due to the interaction between NiS and the host matrix, which facilitates the coalescence of grains. The presence of NiS encourages the formation of larger crystalline domains, enhancing the overall crystallinity of the nanocomposites. The variation in crystallite size highlights the significant impact of thermal treatment and composite formation on the structural evolution of the materials, affecting their properties and potential applications. The performance of the nanocomposites is improved by this structural modification, which also makes them more appropriate for cutting-edge energy applications like solar cells.

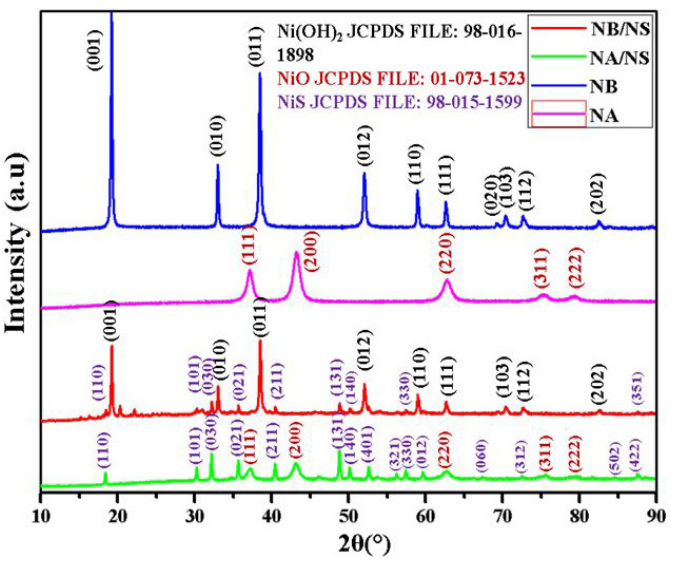


**Fig. 1.** XRD patterns of the as-synthesized samples

**Table 2.** Average value of crystallite sizes of the samples

| *Sample* | *Crystallite size (nm)* |
|---|---|
| NB | 44 |
| NA | 29 |
| NB/NS | 62 |
| NA/NS | 47 |

## UV-Visble Spectroscopy

The optical properties of the samples were investigated using a SHIMADZU UV-2600i UV-Visible spectrometer, and the diffuse reflectance spectroscopy technique was employed to evaluate the samples' optical behavior across a wavelength range of 190-850 nm [Fig. 2(a-d)]. As seen in Fig. 2(a & b), the absorption characteristics of the as-synthesized samples, NB and NA, were predominantly observed in the ultraviolet (UV) region, indicating that both materials possess a high energy bandgap. This is typical for $Ni(OH)_2$ and NiO, which have wide bandgaps that absorb primarily in the UV spectrum. However, when nickel sulfide (NiS) was incorporated into the matrices of $Ni(OH)_2$ and NiO to form the nanocomposites NB/NS and NA/NS, a significant change in the optical absorption behavior was noted. These nanocomposites exhibited absorption extending from the UV region into the visible range, a notable broadening in comparison to the pure materials as seen in Fig. 2(c & d).

There are several reasons for this shift in the absorption spectra, such as the incorporation of sulphur, the existence of structural flaws, electronic modifications, or the formation of new compounds that exhibit altered electronic properties. The extended visible absorption in the nanocomposites suggests that the incorporation of NiS enhanced the ability of these materials to capture photons from a broader portion of the solar spectrum. This improvement in photon absorption is crucial for efficient solar energy harvesting, as it enables the material to make better use of available sunlight. Additionally, the enhanced visible absorption facilitates the generation of more electron-hole pairs, improving the overall photocatalytic and photoelectronic performance of the nanocomposites. Therefore, these NB/NS and NA/NS nanocomposites are particularly promising for solar energy applications, as they can effectively harness a wider range of the solar spectrum, enhancing their efficiency in energy conversion.

Tauc plot analysis is crucial for determining the optical bandgap of materials, particularly semiconductors and nanocomposites. By plotting $(\alpha h\nu)^2$ against $h\nu$, it allows for the estimation of the material's bandgap energy from the linear portion of the curve. This method helps in understanding the material's electronic structure, its potential for optoelectronic applications,

and its suitability for solar energy conversion or photocatalysis based on its ability to absorb light. The Tauc plot equation [47]-[50] is given as follows,

$$\alpha h\nu = \mathrm{A}[h\nu - E_g]^{1/n} \quad ...(2)$$

Here, $\alpha$ refers to the absorption coefficient, A denotes the proportionality constant, $E_g$ depicts the bandgap and the nature of transition is shown by exponent $n$. The Tauc plot analysis yielded useful insights about the optical bandgaps of the synthesised materials, revealing values of 4.4 eV, 3.1 eV, 1.08 eV, and 1.3 eV for NB, NA, NB/NS, and NA/NS, respectively. The significant reduction in bandgap observed in the nanocomposites compared to the pure samples can be attributed to the incorporation of sulphur (S). Sulphur introduces defect states within the crystal structure, which alters the electronic configuration and narrows the energy gap between the conduction and valence bands. This reduction in the bandgap facilitates the absorption of photons in the visible light spectrum, which is typically not possible for materials with wider bandgaps like $Ni(OH)_2$ and NiO. As a result, the nanocomposites (NB/NS and NA/NS) exhibit enhanced light absorption properties, making them more efficient for solar energy applications. The ability to absorb a broader range of light wavelengths improves their potential for energy conversion, particularly for solar cells and other optoelectronic devices.

The refractive index measures how much light is twisted, or refracted, when it travels through a substance. It is crucial for solar cell applications as it affects light absorption, transmission, and reflection at the material interfaces. A higher refractive index can enhance light trapping within the solar cell, increasing the likelihood of photon absorption. Optimizing the refractive index helps improve the efficiency of solar cells by maximizing light capture and minimizing energy losses due to reflection. The refractive indices of the samples were determined using a standard equation [51]-[53] as given by,

$$\frac{n^2-1}{n^2+2} = 1 - \sqrt{\frac{E_g}{20}} \quad ...(3)$$

Here, $n$ depicts the refractive index, while $E_g$ denotes the corresponding band gap. The refractive index values obtained from the analysis were 2.09, 2.36, 3.30, and 3.12 for samples NB, NA, NB/NS, and NA/NS,

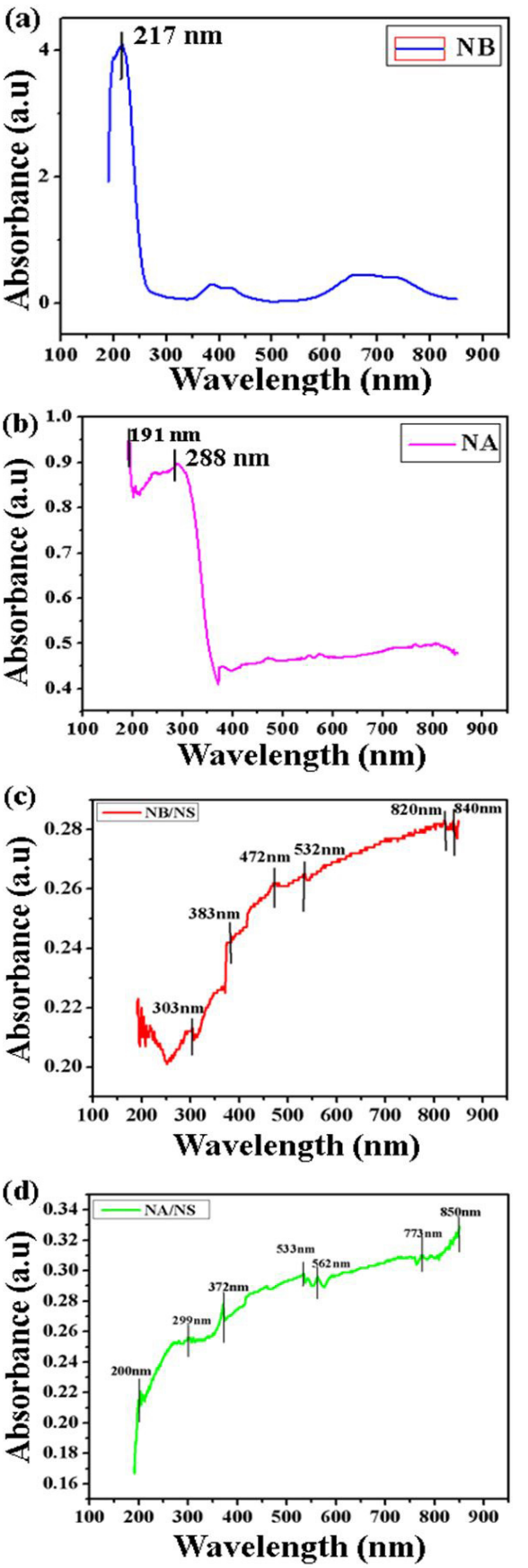


**Fig. 2:** (a-d) Absorption Spectra of the samples

respectively. The higher refractive indices observed for the nanocomposites compared to the pristine samples suggest an increase in optical density, indicating that these materials are more capable of bending light. This enhanced light-trapping capability is particularly beneficial for solar cell applications, as it leads to better photon absorption. A higher refractive index improves the interaction between light and the material, allowing more light to be absorbed rather than reflected. This is essential for maximizing the photon-to-electron conversion efficiency in solar cells.

By reducing reflection losses and increasing the amount of light that enters the material, these nanocomposites offer significant advantages in terms of energy harvesting, making them highly promising candidates for improving the reliability and efficacy of solar energy equipments.

**Morphological Analysis**

FESEM characterization provides an essential tool for studying the surface morphology of materials at the nanoscale level, offering insights into their structural properties. In this study, FESEM analysis was conducted using a JEOL FESEM 7610FPlus model, coupled with EDX spectroscopy to explore the element composition and morphology of the synthesized samples. The results, depicted in Fig. 3(a-d), reveal distinct structural features for each sample. Sample NB, which consists of pure $Ni(OH)_2$, displayed a 2D nanosheet morphology (Fig. 3a). These nanosheets were thin, flat, and interconnected, characteristic of layered materials. This structure is beneficial for improving charge transport and providing a large surface area for interactions with light. Upon calcination to form NiO in sample NA, the nanosheet morphology persisted (Fig. 3b). This stability can be attributed to controlled calcination conditions (temperature and time), which prevented excessive structural rearrangement. Additionally, the inherent stability of $Ni(OH)_2$ nanosheets may have played a role in preserving this morphology during the transformation to NiO. When NiS was incorporated into the matrices to form the nanocomposites, the morphology of the samples changed significantly.

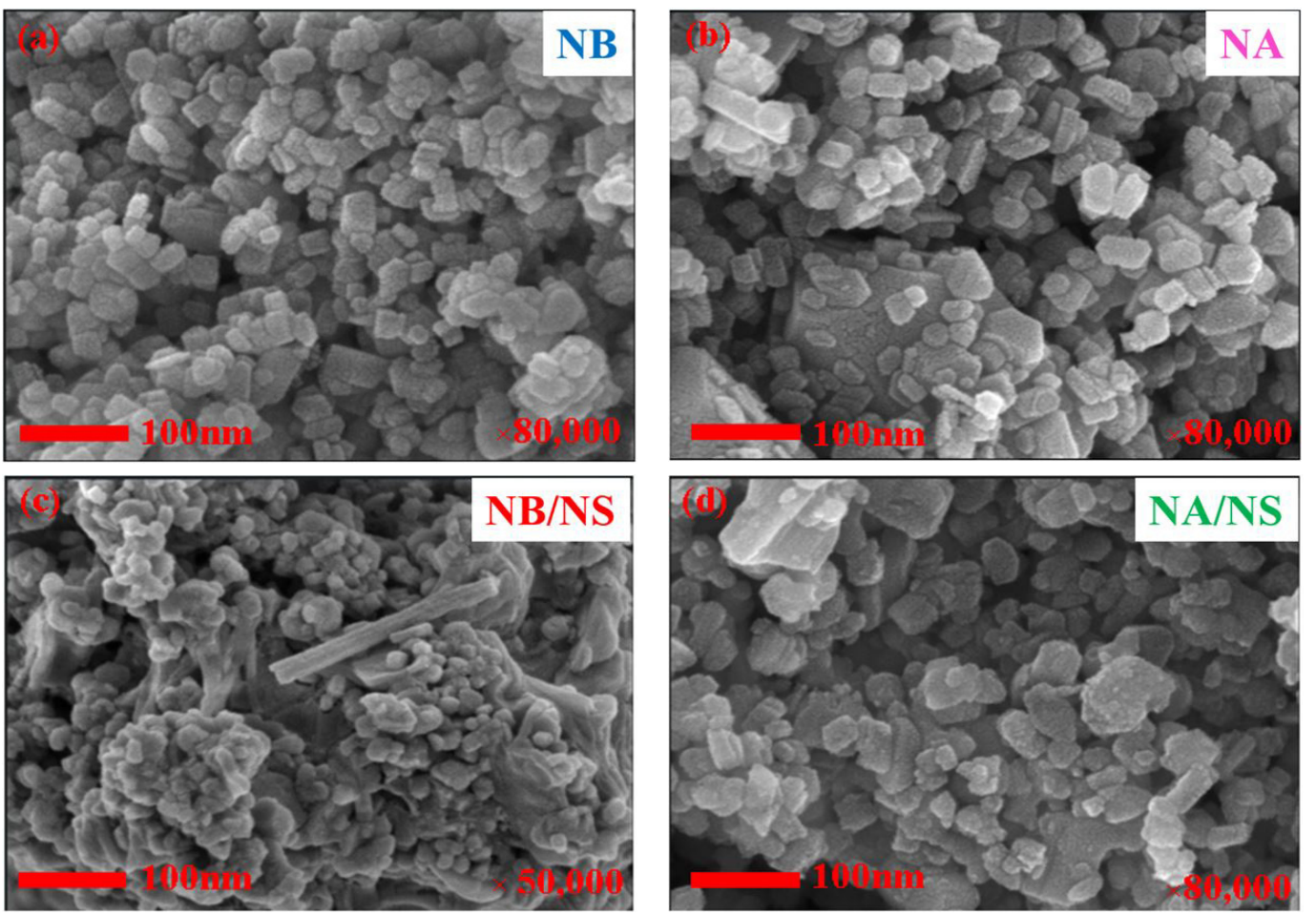

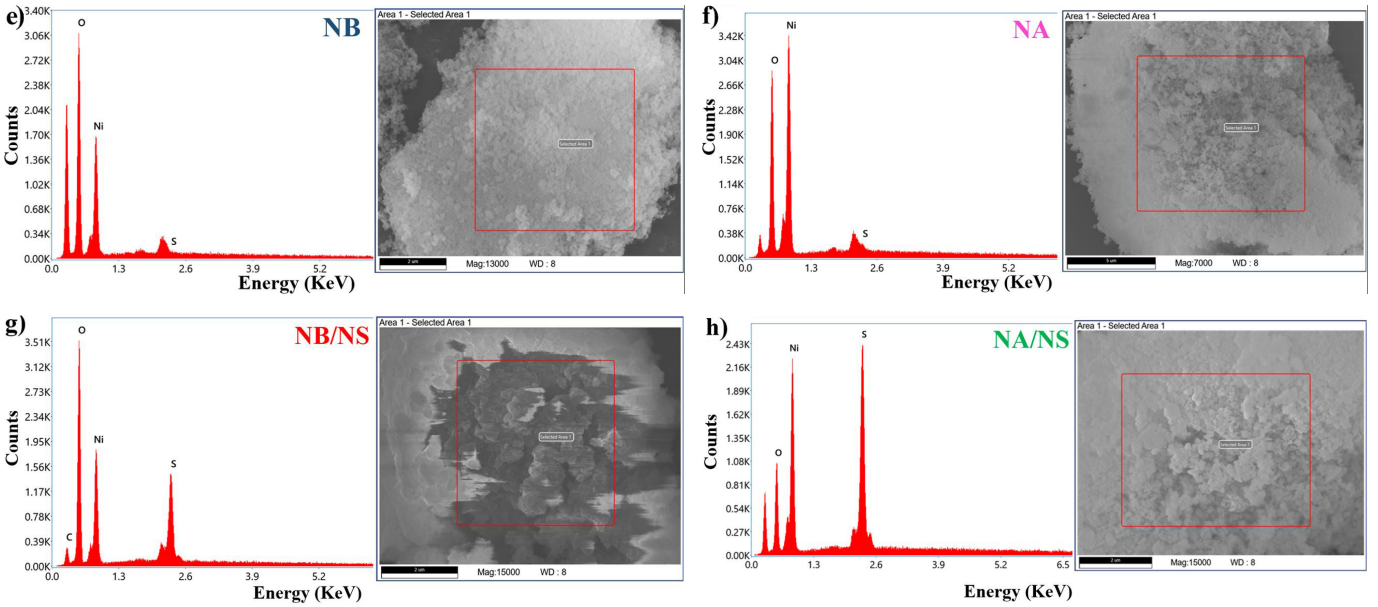


**Fig. 3.** (a-d) FESEM images, (e-h) EDX patterns of the samples

For the NB/NS sample, a broccoli-like structure with intricate branching was observed (Fig. 3c). The development of this unique structure is likely due to the influence of sulphur on the surface energy and crystal growth, which induces the formation of a more complex network. This branching morphology increases the material's surface area and facilitates better charge transport and light absorption, both of which are crucial for enhancing the efficacy of solar cells.

In the NA/NS scenario, the incorporation of NiS led to a shift in morphology to clustered 2D nanosheets (Fig. 3d). The presence of sulphur likely played a significant role in altering the growth processes, leading to this new structure. The clustered morphology enhances surface interaction, which is critical for efficient charge separation in solar cell applications. These changes in morphology, induced by the incorporation of NiS, are expected to improve the overall performance of the nanocomposites, making them more suitable for use in high-performance solar cells.

EDX analysis, shown in fig. 3(e-h), was used to verify the elemental composition of the samples. For samples NB and NA, the EDX spectra revealed distinct peaks for nickel (Ni) and oxygen (O), indicating the presence of $Ni(OH)_2$ and NiO in these respective samples. This was consistent with the expected composition of these materials. In contrast, for the nanocomposites NB/NS and NA/NS, the EDX spectra showed additional peaks for sulphur (S), confirming the successful incorporation of NiS into the matrices of $Ni(OH)_2$ and NiO. The presence of sulphur in the nanocomposites further supports the formation of the $Ni(OH)_2$/NiS and NiO/NiS composite structures. Carbon peaks were also observed in all the samples, which originated from the carbon tape used during the EDX analysis. These findings validated the effective synthesis of the intended nanocomposites and offered insightful information on the elemental composition.

## Chemical Analysis

The Fourier Transform Infrared Spectroscopy (FTIR) analysis was utilised to study the bond formations and functional groups existing in the synthesized samples. The FTIR spectra were recorded using the FT-IR Spectrum 2 spectrometer from Perkin Elmer, spanning a wavenumber range of 4000–500 $cm^{-1}$. The resulting spectra are shown in fig. 4. For the pure nickel-based samples, broad peaks at 3404 $cm^{-1}$, 3424 $cm^{-1}$, and 3439 $cm^{-1}$ were observed in samples NB, NA, and NA/NS, respectively. These peaks are characteristic of O-H stretching vibrations, which are likely attributed to absorbed water molecules on the surfaces of the samples [54],[55]. The presence of these O-H stretching bands is a common feature in metal hydroxides, where water molecules interact with the surface [56]. In the NB/NS sample, this O-H stretching band was found to shift slightly to 3627 $cm^{-1}$, suggesting a stronger hydrogen

bonding interaction or a change in the local chemical environment caused by the incorporation of NiS into the matrix.

Additionally, all samples exhibited weak bands in the range of 3000–2800 $cm^{-1}$, indicating the presence of C-H stretching vibrations [57], which are likely from organic residues or impurities in the samples. The presence of carbon-containing groups was further supported by the moderate peaks observed around 1739 $cm^{-1}$ for NB/NS and 1706 $cm^{-1}$ for NA/NS, which are indicative of C=O stretching vibrations [58]. This may be attributed to the carbonyl groups in surface residues or adsorbed organic molecules.

A noticeable shift in the peaks corresponding to C=C stretching vibrations [59] was observed in samples NA, NB, and NA/NS, with bands ranging from 1627 $cm^{-1}$ to 1635 $cm^{-1}$. These shifts could be associated with changes in the electronic environment around the carbon-carbon bonds, possibly due to the presence of structural defects or interactions with other components in the samples. The peaks between 1375 $cm^{-1}$ and 1150 $cm^{-1}$ are attributed to C-O stretching vibrations, further affirming the existence of carbon-oxygen bonds, likely from organic contaminants or adsorbed species.

One of the most distinctive features in the FTIR spectra of the nanocomposites is the peak observed at 675 $cm^{-1}$ in the NB/NS sample, which corresponds to C=S stretching vibrations. This peak is a clear indication of the incorporation of sulphur into the nanocomposite, confirming the successful synthesis of the $Ni(OH)_2$/NiS and NiO/NiS nanocomposite structures. The presence of C=S stretching vibrations further supports the formation of nickel-sulphide interactions within the nanocomposite.

In the fingerprint region of the FTIR spectra, a sharp and prominent peak was observed at 522 $cm^{-1}$ in the NB/NS sample, which corresponds to Ni-O vibrations [60], confirming the presence of nickel-oxide bonds in the material. A broad peak at 539 $cm^{-1}$ was also noticed in sample NB, which can be attributed to Ni-OH stretching vibrations [61], demonstrating the existence of hydroxyl groups in the $Ni(OH)_2$ phase. Lastly, for all samples, peaks between 435 $cm^{-1}$ and 419 $cm^{-1}$ were observed, corresponding to Ni-O vibrations [62], which is a signature feature of nickel oxide bonds, confirming the formation of nickel oxide in the synthesized materials. These FTIR results provide detailed insights into the chemical bonding and functional groups existing in the materials, supporting the successful synthesis of the nickel-based nanocomposites with NiO and NiS incorporation.

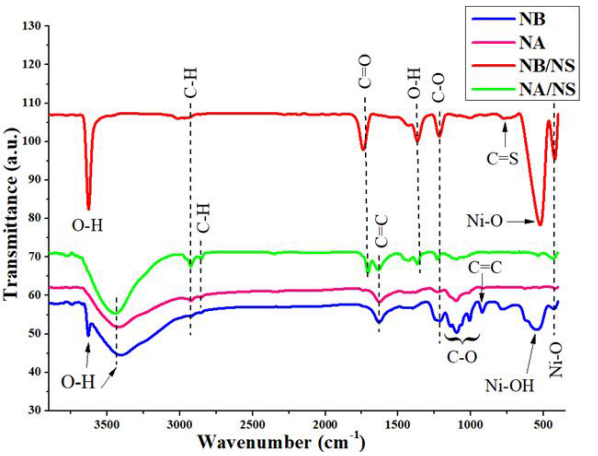


**Fig. 4.** FTIR spectra of the samples

## CONCLUSION

The present study successfully demonstrated the hydrothermal synthesis and characterization of $Ni(OH)_2$, NiO, and their respective nanocomposites with nickel sulfide (NiS), targeting advanced solar energy applications. XRD analysis affirmed the effective formation of hexagonal $Ni(OH)_2$, NiS, and cubic NiO phases, showcasing well-defined crystalline structures of the samples. FESEM highlighted distinct morphologies, with $Ni(OH)_2$ and NiO maintaining nanosheet-like structures, while the nanocomposites exhibited a unique broccoli-like morphology, enhancing surface area and providing more active sites for interactions. Optical analysis via UV-Visible spectroscopy indicated a significant reduction in the band gap values from 4.4 eV and 3.1 eV for pure $Ni(OH)_2$ and NiO, respectively, to 1.08 eV and 1.3 eV in the $Ni(OH)_2$/NiS and NiO/NiS nanocomposites. This bandgap reduction is essential because it allows the materials to absorb a wider range of light, especially visible light, which is essential for improving the efficiency of solar energy harvesting.

The integration of NiS with $Ni(OH)_2$ and NiO results in a synergistic effect that improves the optical and electronic properties of the materials, addressing the limitations often observed in their standalone counterparts. This combination not only improves visible light absorption but also promotes better charge

carrier mobility, an essential factor in enhancing the overall efficiency of solar energy conversion. Additionally, the nanocomposites exhibited an excellent balance of stability and enhanced electronic characteristics, making them promising candidates for use in solar cells. These findings emphasize the potential of nickel-based nanocomposites as cost-effective, environmentally friendly alternatives to conventional materials in solar energy applications.

This research highlights the importance of material engineering strategies to tailor properties for sustainable energy solutions. The ability to fine-tune these properties opens avenues for further optimization in solar cell design. Future studies could explore the integration of these nanocomposites into working solar cell prototypes to assess their practical performance, long-term stability, and scalability, thus supporting the development of sustainable, effective energy technologies. Additionally, further characterization techniques like cyclic voltammetry (CV), electrochemical impedance spectroscopy (EIS), and electrochemical charge-discharge tests could be employed to assess the charge storage capacity, electrochemical stability, and efficiency of these nanocomposites in energy storage and conversion systems. These methods will provide a deeper understanding of the materials' behavior under different electrochemical conditions, ensuring their reliability and performance in practical applications. Thin-film deposition techniques, such as spin coating or sputtering, can also be explored to fabricate thin-film solar cells, providing insights into their scalability and efficiency for large-scale applications. This would enable better integration into photovoltaic devices, enhancing their commercial viability.

## ACKNOWLEDGMENTS

The authors gratefully acknowledge essential resources provided by Prof. Anand Srivastava, Hon. Vice Chancellor of Netaji Subhas University of Technology (former Netaji Subhas Institute of Technology, University of Delhi).

## DECLARATION OF COMPETING INTEREST

The authors confirm that no financial conflicts or personal relationships exist that could have impacted the research presented in this paper.

## ETHICAL APPROVAL

All the authors have worked in accordance with the ethical standards and approved by Netaji Subhas University of Technology.

## REFERENCES

[1] L. M. Shaker, A. A. Al-Amiery, M. M. Hanoon, W. K. Al-Azzawi, and A. A. H. Kadhum, "Examining the influence of thermal effects on solar cells: a comprehensive review," *Sustainable Energy Research* 2024 11:1, vol. 11, no. 1, pp. 1–30, Feb. 2024, doi: 10.1186/S40807-024-00100-8.

[2] P. Phogat, S. Shreya, R. Jha, and S. Singh, "Impedance Study of Zinc Sulphide Quantum Dots via One Step Green Synthesis," *Materials Science Forum*, vol. 1099, pp. 119–125, Oct. 2023, doi: 10.4028/P-G1CCXQ.

[3] Dipti, P. Phogat, Shreya, D. Kumari, and S. Singh, "Fabrication of tunable band gap carbon based zinc nanocomposites for enhanced capacitive behaviour," *Phys Scr*, vol. 98, no. 9, Sep. 2023, doi: 10.1088/1402-4896/ACF07B.

[4] P. Phogat, Shreya, R. Jha, and S. Singh, "Optical and Microstructural Study of Wide Band Gap ZnO@ ZnS Core–Shell Nanorods to be Used as Solar Cell Applications," pp. 419–429, 2023, doi: 10.1007/978-981-99-2349-6_38.

[5] Shreya, P. Phogat, R. Jha, and S. Singh, "Elevated Refractive Index of MoS2 Amorphous Nanoparticles with a Reduced Band Gap Applicable for Optoelectronics," pp. 431–439, 2023, doi: 10.1007/978-981-99-2349-6_39.

[6] T. Kumar, Shreya, P. Phogat, V. Sahgal, and R. Jha, "Surfactant-mediated modulation of morphology and charge transfer dynamics in tungsten oxide nanoparticles," *Phys Scr*, vol. 98, no. 8, Aug. 2023, doi: 10.1088/1402-4896/ACE566.

[7] S. Rai, Shreya, P. Phogat, R. Jha, and S. Singh, "Hydrothermal synthesis and characterization of selenium-doped MoS 2 for enhanced optoelectronic properties," *MATEC Web of Conferences*, vol. 393, p. 01008, Mar. 2024, doi: 10.1051/MATECCONF/202439301008.

[8] S. Sharma, P. Phogat, R. Jha, and S. Singh, "Electrochemical and Optical Properties of Microwave Assisted MoS2 Nanospheres for Solar Cell Application," *International Journal of Smart Grid and Clean Energy*, pp. 66–72, 2023, doi: 10.12720/SGCE.12.3.66-72.

[9] Shreya, P. Phogat, R. Jha, and S. Singh, "Microwave-synthesized γ-WO3 nanorods exhibiting high current density and diffusion characteristics," *Transition Metal Chemistry*, vol. 48, no. 3, pp. 167–183, Jun. 2023, doi: 10.1007/S11243-023-00533-Y.

[10] P. Phogat, Shreya, R. Jha, and S. Singh, "Diffusion Controlled Features of Microwave Assisted ZnS/ZnO Nanocomposite with Reduced Band Gap," *ECS Journal of Solid State Science and Technology*, vol. 12, no. 3, p. 034004, Mar. 2023, doi: 10.1149/2162-8777/ACC426.

[11] P. PHOGAT, . S., R. JHA, and S. Singh, "Electrochemical Analysis of Thermally Treated Two Dimensional Zinc Sulphide Hexagonal Nano-Sheets with Reduced Band Gap," *Phys Scr*, Dec. 2023, doi: 10.1088/1402-4896/AD0D93.

[12] D. Kumari, Shreya, P. Phogat, Dipti, S. Singh, and R. Jha, "Enhanced electrochemical behavior of C@CdS Core-Shell heterostructures," *Materials Science and Engineering: B*, vol. 301, p. 117212, Mar. 2024, doi: 10.1016/J.MSEB.2024.117212.

[13] P. Phogat, Shreya, R. Jha, and S. Singh, "Phase Transition of Thermally Treated Polyhedral Nano Nickel Oxide with Reduced Band Gap," *MATEC Web of Conferences*, vol. 393, p. 01001, Mar. 2024, doi: 10.1051/MATECCONF/202439301001.

[14] E. R. Beach, K. Shqau, S. E. Brown, S. J. Rozeveld, and P. A. Morris, "Solvothermal synthesis of crystalline nickel oxide nanoparticles," *Mater. Chem. Phys.*, vol. 115, no. 1, p. 371, May 2009, doi: 10.1016/j.matchemphys.2008.12.018.

[15] Q. Yang, J. Sha, X. Ma, and D. Yang, "Synthesis of NiO nanowires by a sol-gel process," *Mater. Lett.*, vol. 59, no. 14–15, p. 1967, Jun. 2005, doi: 10.1016/j.matlet.2005.02.037.

[16] P. Palanisamy and A. M. Raichur, "Synthesis of spherical NiO nanoparticles through a novel biosurfactant mediated emulsion technique," *Mater. Sci. Eng. C.*, vol. 29, no. 1, p. 199, Jan. 2009, doi: 10.1016/j.msec.2008.06.008.

[17] E. Shangguan, Z. Chang, H. Tang, X. Z. Yuan, and H. Wang, "Synthesis and characterization of high-density non-spherical Ni(OH)2 cathode material for Ni–MH batteries," *Int J Hydrogen Energy*, vol. 35, no. 18, pp. 9716–9724, Sep. 2010, doi: 10.1016/J.IJHYDENE.2010.06.096.

[18] D. S. Hall, D.J. Lockwood, C. Bock, and B.R. MacDougall, "Nickel hydroxides and related materials: a review of their structures, synthesis and properties," *Proceedings of the Royal Society A: Mathematical, Physical and Engineering Sciences*, vol. 471, no. 2174, Feb. 2015, doi: 10.1098/RSPA.2014.0792.

[19] L. Zhang et al., "$Ni(OH)_2$ nanoparticles encapsulated in conductive nanowire array for high-performance alkaline seawater oxidation," *Nano Res*, vol. 15, no. 7, pp. 6084–6090, Jul. 2022, doi: 10.1007/S12274-022-4391-6/METRICS.

[20] J. Ji et al., "Nanoporous $Ni(OH)_2$ thin film on 3D ultrathin-graphite foam for asymmetric supercapacitor," *ACS Nano*, vol. 7, no. 7, pp. 6237–6243, Jul. 2013, doi: 10.1021/nn4021955.

[21] H. B. Li et al., "Amorphous nickel hydroxide nanospheres with ultrahigh capacitance and energy density as electrochemical pseudocapacitor materials," *Nat. Commun.*, vol. 4, p. 1894, 2012, doi: 10.1038/ncomms2932.

[22] R. Wang, J. Lang, Y. Liu, Z. Lin, and X. Yan, "Ultra-small, size-controlled Ni(OH)2 nanoparticles: elucidating the relationship between particle size and electrochemical performance for advanced energy storage devices," *NPG Asia Materials 2015*, vol. 7, no. 6, pp. e183–e183, Jun. 2015, doi: 10.1038/am.2015.42.

[23] R. Goel, R. Jha, and C. Ravikant, "Investigating the structural, electrochemical, and optical properties of p-type spherical nickel oxide (NiO) nanoparticles," *Journal of Physics and Chemistry of Solids*, vol. 144, p. 109488, Sep. 2020, doi: 10.1016/J.JPCS.2020.109488.

[24] Y. Xia et al., "One-dimensional nanostructures: Synthesis, characterization, and applications," *Adv. Mater.*, vol. 15, no. 5, p. 353, Mar. 2003, doi: 10.1002/adma.200390087.

[25] G. J. Li, X. X. Huang, Y. Shi, and J. K. Guo, "Preparation and characteristics of nanocrystalline NiO by organic solvent method," *Mater. Lett.*, vol. 51, no. 4, p. 325, Nov. 2001, doi: 10.1016/s0167-577x(01)00312-3.

[26] M. Alagiri, S. Ponnusamy, and C. Muthamizhchelvan, "Synthesis and characterization of NiO nanoparticles by sol-gel method," *Journal of Materials Science: Materials in Electronics*, vol. 23, no. 3, pp. 728–732, Mar. 2012, doi: 10.1007/S10854-011-0479-6/FIGURES/8.

[27] F. J. Morin, "Electrical Properties of NiO," *Physical Review*, vol. 93, no. 6, pp. 1199–1204, 1954, doi: 10.1103/PhysRev.93.1199.

[28] A. Sharma, P.R. Makgwane, E. Lichtfouse, N. Kumar, A. H. Bandegharaei, and M. Tahir, "Recent advances in synthesis, structural properties, and regulation of nickel sulfide-based heterostructures for environmental water remediation: An insight review," *Environmental Science and Pollution Research 2023*, vol. 30, no. 24, pp. 64932–64948, Apr. 2023, doi: 10.1007/S11356-023-27093-Z.

[29] Y. Chen, Y. Cheng, T. Zhang, H. Zhang, and S. Zhong, "Photodeposition of NiS thin film enhanced the visible light hydrogen evolution performance of CdS nanoflowers," *Int J Hydrogen Energy*, vol. 77, pp. 184–192, Aug. 2024, doi: 10.1016/J.IJHYDENE.2024.06.130.

[30] R. Boughalmi, R. Rahmani, A. Boukhachem, B. Amrani, K. Driss-Khodja, and M. Amlouk, "Metallic behavior of NiS thin film under the structural, optical, electrical and ab initio investigation frameworks," *Mater Chem*

*Phys*, vol. 163, pp. 99–106, Aug. 2015, doi: 10.1016/J.MATCHEMPHYS.2015.07.019.

[31] M. Mollavali, C. Falamaki, and S. Rohani, "Efficient light harvesting by NiS/CdS/ZnS NPs incorporated in C, N-co-doped-TiO2 nanotube arrays as visible-light sensitive multilayer photoanode for solar applications," *Int J Hydrogen Energy*, vol. 43, no. 19, pp. 9259–9278, May 2018, doi: 10.1016/J.IJHYDENE.2018.03.102.

[32] D. Wang, M. Wright, N. K. Elumalai, and A. Uddin, "Stability of perovskite solar cells," *Solar Energy Materials and Solar Cells*, vol. 147, pp. 255–275, Apr. 2016, doi: 10.1016/J.SOLMAT.2015.12.025.

[33] H. S. Jung and N. G. Park, "Perovskite Solar Cells: From Materials to Devices," *Small*, vol. 11, no. 1, pp. 10–25, Jan. 2015, doi: 10.1002/SMLL.201402767.

[34] M. A. Green, A. Ho-Baillie, and H. J. Snaith, "The emergence of perovskite solar cells," *Nature Photonics 2014*, vol. 8, no. 7, pp. 506–514, Jun. 2014, doi: 10.1038/nphoton.2014.134.

[35] S. Emin, S. P. Singh, L. Han, N. Satoh, and A. Islam, "Colloidal quantum dot solar cells," *Solar Energy*, vol. 85, no. 6, pp. 1264–1282, Jun. 2011, doi: 10.1016/J.SOLENER.2011.02.005.

[36] A. J. Nozik, "Quantum dot solar cells," *Physica E Low Dimens Syst Nanostruct*, vol. 14, no. 1–2, pp. 115–120, Apr. 2002, doi: 10.1016/S1386-9477(02)00374-0.

[37] Z. Yang et al., "Mixed-quantum-dot solar cells," *Nature Communications 2017*, vol. 8, no. 1, pp. 1–9, Nov. 2017, doi: 10.1038/s41467-017-01362-1.

[38] L. Hrostea, M. Boclinca, M. Socol, L. Leontie, A. Stanculescu, and M. Girtan, "Oxide/metal/oxide electrodes for solar cell applications," Solar Energy, vol. 146, pp. 464–469, Apr. 2017, doi: 10.1016/J.SOLENER.2017.03.017.

[39] R. Jose, V. Thavasi, and S. Ramakrishna, "Metal Oxides for Dye-Sensitized Solar Cells," *Journal of the American Ceramic Society*, vol. 92, no. 2, pp. 289–301, Feb. 2009, doi: 10.1111/J.1551-2916.2008.02870.X.

[40] Q. Zhang, C. S. Dandeneau, X. Zhou, and C. Cao, "ZnO Nanostructures for Dye-Sensitized Solar Cells," *Advanced Materials*, vol. 21, no. 41, pp. 4087–4108, Nov. 2009, doi: 10.1002/ADMA.200803827.

[41] Z. Yue, H. Guo, and Y. Cheng, "Toxicity of Perovskite Solar Cells," *Energies 2023*, Vol. 16, Page 4007, vol. 16, no. 10, p. 4007, May 2023, doi: 10.3390/EN16104007.

[42] S. S. Kanmani and K. Ramachandran, "Synthesis and characterization of $TiO_2$/ZnO core/shell nanomaterials for solar cell applications," *Renew Energy*, vol. 43, pp. 149–156, Jul. 2012, doi: 10.1016/J.RENENE.2011.12.014.

[43] Shreya, S. Rai, P. Phogat, R. Jha, and S. Singh, "Synergistic effects of Carbon@MoS2 core-shell nanostructures on charge dynamics for future optoelectronic applications," *Mater Chem Phys*, vol. 329, p. 130147, Jan. 2025, doi: 10.1016/J.MATCHEMPHYS.2024.130147.

[44] P. Phogat, S. Rai, Shreya, R. Jha, and S. Singh, "High-performance self-powered electrochemical photodetectors based on co-precipitation and hydrothermally synthesized HgS nanoparticles," *Journal of Materials Science: Materials in Electronics*, vol. 35, no. 22, pp. 1–15, Aug. 2024, doi: 10.1007/S10854-024-13299-5/METRICS.

[45] Shreya, P. Phogat, R. Jha, and S. Singh, "Carbon nanospheres-induced enhanced capacitive dynamics in C/WS2/WO3 nanocomposites for high-performance electrochemical capacitors," *Materials Science and Engineering: B*, vol. 304, Jun. 2024, doi: 10.1016/J.MSEB.2024.117390.

[46] N. Shreya, P. Phogat, R. Jha, and S. Singh, "Enhanced Electrochemical Performance and Charge-Transfer Dynamics of 2D MoS2/WO3 Nanocomposites for Futuristic Energy Applications," *ACS Appl Nano Mater*, vol. 7, no. 8, pp. 8593–8611, Apr. 2024, doi: 10.1021/ACSANM.3C06017/SUPPL_FILE/AN3C06017_SI_001.PDF.

[47] S. Rai, Shreya, P. Phogat, R. Jha, and S. Singh, "Wide absorption spectrum and rapid response time of PEC photodetectors based on MoS2–Se nanocomposites," *Chem Eng Commun*, pp. 1–16, Jun. 2024, doi: 10.1080/00986445.2024.2362799.

[48] Shreya, P. Phogat, R. Jha, and S. Singh, "Electrochemical study of cerium and iron doped MoO3 nanoparticles showing potential for supercapacitor application," *Next Materials*, vol. 5, p. 100260, Oct. 2024, doi: 10.1016/J.NXMATE.2024.100260.

[49] P. Phogat, Shreya, R. Jha, and S. Singh, "Synthesis and characterization of C@CdS core-shell structures for high-performance capacitors," *Next Materials*, vol. 5, p. 100246, Oct. 2024, doi: 10.1016/J.NXMATE.2024.100246.

[50] T. Jindal, P. Phogat, Shreya, S. Singh, and R. Jha, "Electrochemical and optical comparison of Cr3+, Co2+, Ag1+, Hg1+ and Pb4+ doped WO3 as a thin layer working electrode for electrochemical sensing," *Appl Phys A Mater Sci Process*, vol. 130, no. 7, Jul. 2024, doi: 10.1007/S00339-024-07666-6.

[51] P. Phogat, Shreya, R. Jha, and S. Singh, "Supercapacitive studies of hybrid materials based on cadmium deuteroxide chloride (CdDOCl) with activated carbon," *J Mater Sci*, vol. 59, no. 26, pp. 11757–11780, Jul. 2024, doi: 10.1007/S10853-024-09874-0/FIGURES/10.

[52] V. Sahgal, P. Phogat, Shreya, T. Kumar, R. Jha, and S. Singh, "Design strategies for morphologically ramified ZnO–ZnS core shell nano flowers for magnified electrochemical studies," *Indian Journal of Physics*, pp.

1–22, May 2024, doi: 10.1007/S12648-024-03196-2/METRICS.

[53] P. Phogat, Shreya, R. Jha, and S. Singh, "Photocatalytic Performance of ZnO@ZnS Core–Shell Heterostructures for Malachite Green and Rhodamine B Dye Degradation," *Physica status solidi* (a), p. 2400404, 2024, doi: 10.1002/PSSA.202400404.

[54] Shreya, P. Phogat, R. Jha, and S. Singh, "Electrochemical analysis of hydrothermally synthesized 2D/1D WS2/WO3 nanocomposites for solar cell application," *Journal of Physics and Chemistry of Solids*, vol. 192, p. 112110, Sep. 2024, doi: 10.1016/J.JPCS.2024.112110.

[55] P. Phogat, Shreya, R. Jha, and S. Singh, "Synthesis of novel ZnO nanoparticles with optimized band gap of 1.4 eV for high-sensitivity photo electrochemical detection," *Materials Today Sustainability*, vol. 27, p. 100823, Sep. 2024, doi: 10.1016/J.MTSUST.2024.100823.

[56] P. Phogat, Shreya, R. Jha, and S. Singh, "Supercapacitive studies of hybrid materials based on cadmium deuteroxide chloride (CdDOCl) with activated carbon," *J Mater Sci*, Jul. 2024, doi: 10.1007/S10853-024-09874-0.

[57] Shreya, P. Phogat, S. Singh, and R. Jha, "Reduction mechanism of hydrothermally synthesized wide band gap ZnWO 4 nanorods for HER application," *MATEC Web of Conferences*, vol. 393, p. 01004, Mar. 2024, doi: 10.1051/MATECCONF/202439301004.

[58] P. Phogat, Shreya, R. Jha, and S. Singh, "Design and performance evaluation of 2D nickel oxide nanosheet thin film electrodes in energy storage devices," *Indian Journal of Physics*, 2024, doi: 10.1007/S12648-024-03415-W.

[59] S. Shreya, P. Phogat, R. Jha, and S. Singh, " Effect of Heterojunction Dynamics on Charge Transfer Mechanism in Type-II ZnS/MoS 2 Nanocomposite," *ECS Meeting Abstracts*, vol. MA2024-01, no. 54, pp. 2894–2894, Aug. 2024, doi: 10.1149/MA2024-01542894MTGABS.

[60] A. Rahdar, M. Aliahmad, and Y. Azizi, "NiO Nanoparticles: Synthesis and Characterization," *Journal of Nanostructures*, vol. 5, no. 2, pp. 145–151, Apr. 2015, doi: 10.7508/JNS.2015.02.009.

[61] D. P. Dubal, V.J. Fulari, and C.D. Lokhande, "Effect of morphology on supercapacitive properties of chemically grown β-Ni(OH)2 thin films," *Microporous and Mesoporous Materials*, vol. 151, pp. 511–516, Mar. 2012, doi: 10.1016/J.MICROMESO.2011.08.034.

[62] O. O. Balayeva et al., "β-NiS and Ni3S4 nanostructures: Fabrication and characterization," *Mater Res Bull*, vol. 75, pp. 155–161, Mar. 2016, doi: 10.1016/J.MATERRESBULL.2015.11.037.